communications earth & environment

ARTICLE

https://doi.org/10.1038/s43247-023-01096-7 OPEN

Circulation dampened heat extremes intensification over the Midwest USA and amplified over Western Europe

Jitendra Singh [1✉], Sebastian Sippel[1,2] & Erich M. Fischer [1]

Globally heat extremes have intensified in recent decades. However, while Western Europe shows a remarkably strong intensification of heat extremes, the Midwest United States experienced only weak warming of warmest nighttime and even a weak decrease in the intensity of daytime heat extremes since 1979. Here, we show that for daytime heat extremes in the Midwest United States atmospheric circulation induced ~1 °C cooling since 1979, reversing the thermodynamic warming trend. The observed circulation-induced trend is outside the multi-model range and the overall trend at the very low end of it. In Western Europe circulation greatly amplified warming by ~1 °C, accounting to one third of observed trend. The observed circulation- and thermodynamic-induced trends, as well as the total observed trends are at the high end of the model range in Western Europe. Understanding whether the strong circulation-induced trends are externally forced or unforced internal variability remains key to constrain future trends in heat extremes.

[1] Institute for Atmospheric and Climate Science, ETH Zurich, Zurich, Switzerland. [2] Leipzig Institute for Meteorology, Leipzig University, Leipzig, Germany. ✉email: jitendra.singh@env.ethz.ch

Earth's global average near-surface air temperature in 2011-2020 has increased by 1.1 °C (0.9−1.3 °C) since the pre-industrial period due to anthropogenic forcings[1], leading to an increase in heat extremes on a regional and a global scale[2–4]. However, some regions have experienced disproportionate changes in heat extremes in recent decades—such as the Midwest USA (MUS), which has experienced a weak decreasing trend in the intensity of heat extremes since 1951 (Fig. 1 and Supplementary Fig. 1). In contrast, Western Europe (WEU) has experienced a remarkable increase of over 3 °C in the intensity of heat extremes since 1951, thus outpacing global-mean temperature change. It remains largely unclear as to why these regions experience opposite heat extreme trends, and in fact, this has been one of the most intriguing and less understood questions among the climate science community[5].

The MUS experiences a weak cooling trend in heat extremes despite moderate warming of daily average summer temperature across the region[6], referred to as a "warming hole"[7]. Several studies attribute this long-term cooling trend to large-scale ocean-atmospheric patterns[8], increased irrigation[9,10], regional reforestation[11], and aerosol changes[7]. Notably, Mueller et al.[9] show that heavy irrigation activities lead to cooler temperatures by enhancing evapotranspiration-driven cooling over the MUS. However, it remains unclear to what extent the trends over the MUS are caused by anthropogenic forcings or unforced internal variability[12,13]. In contrast, WEU has been identified as a heat wave hotspot[14–18] with a faster warming rate than many other parts of the world in the last four decades[19–21]. In boreal summer, northern high-latitude land warming provides favorable conditions for forming blocking anticyclones[22], a primary driver of heat extremes over WEU[19,23]. Besides anthropogenic global warming, observational and model-based studies attribute the WEU warming to a decline in aerosol forcing and cloud cover[24,25], changes in atmospheric circulation states[26–28], including the increase in frequency and persistence of the midlatitude jet stream[19]. Additionally, local factors such as soil moisture deficit and related land-atmosphere feedback mechanisms contribute to the further intensification of heat extremes over WEU[29,30].

Unforced internal variability in the climate system can also substantially alter the warming rate in different regions across the globe[31]. For example, previous studies suggest a strong effect of internal variability on the MUS summer temperature[10,32] and on the North American climate as a whole[33]. In addition, the relative magnitude of internal variability is larger on shorter time scales, and may thus manifest itself more strongly on time scales of weekly or sub-weekly temperature extremes[34]. Likewise, previous studies highlight the role of basin-scale changes in the Atlantic multidecadal variations in the WEU summer climate[18,35]. Both internal variability and local external forcings broadly manifest their influence on regional warming by altering the atmospheric circulation states through various mechanisms, including regional teleconnections, the midlatitude jet stream, and land-atmosphere feedback[31].

This study aims to understand why the observed trends in heat extremes intensity over the MUS and WEU are remarkably low and high, respectively, and what they imply for the future. We specifically chose these two regions due to their unusual trends, which are not representative of many other regions where the observed trends fall well within the range of models. We use observations of circulation and temperature, as well as Earth System Model (ESM) large ensemble simulations to examine how circulation-induced changes in heat extremes explain the observed exceptional warming trend over WEU and cooling trend over the MUS. Understanding observed trends and related physical processes would be crucial to constrain future change in heat extremes[36], and thus to design adaptation and resilience plans. Our analysis comprises a dynamical adjustment approach[28,31,37], which is used to disentangle the contribution of circulation-

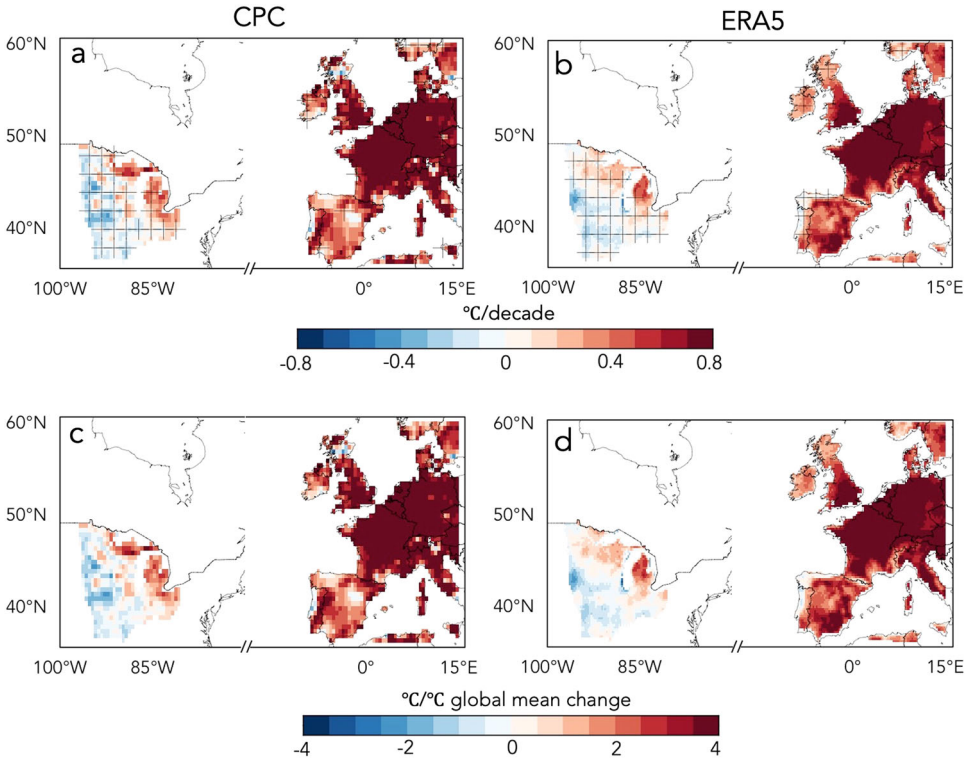

Fig. 1 Observed Tx5d trends. a, **b** Spatial distribution of trends in the intensity of Tx5d in CPC and ERA5 reanalysis in the MUS and in WEU during 1979–2021. The hatching indicates statistically insignificant trends at a 10% significance level. **c**, **d** Same as panels **a**, **b** but show Tx5d trends relative to changes in global-mean surface temperature. The trends and their statistical significance are calculated using Theil-Sen's slope estimator.

induced changes and forced changes resulting from all other forcings combined to observed trends in these regions.

Results

Contrasting trends in the intensity of heat extremes over the MUS and WEU. Observational analysis shows a remarkable increasing trend in the intensity (referred to as warming trend hereafter) of the annual hottest five-day period (Tx5d) across WEU and a weak decreasing trend in the intensity (referred to as cooling trend hereafter) of Tx5d over a large portion of the MUS during 1979–2021 (Fig. 1) and 1951–2021 (Fig. S1). Despite variations in the trend amplitudes, the pattern of opposite trends in these regions is consistent across observational datasets and insensitive to the exact time horizon considered in trend estimation (Fig. 1a, b and Supplementary Fig. 1). Tx5d intensity over MUS has cooled slightly over the last four decades. This cooling trend is notable, given that the warmest 5 consecutive nights (defined as a 5-day average of daily minimum temperature; Tn5d) (Supplementary Fig. 2a) as well as, the corresponding average temperature over the MUS[6] as well as heat extremes nearly anywhere else in the world have been warming during the same period. Within the MUS region the cooling trends in Tx5d are most pronounced over the western MUS, and offset the weak warming trends in other parts of the MUS. Averaged across MUS they result in an overall weak cooling trend of Tx5d since 1979.

Notably, the MUS cooling is more pronounced in shorter-duration heat extremes. For instance, annual maximum temperature intensity (TXx) show strongest cooling trends of ~0.7 °C in the past four decades, corresponding to a cooling rate of ~1 °C for each °C of global-mean surface temperature (GMST) warming, while the intensity of annual hottest 15-day period (Tx15d) exhibit a very weak warming trend (Supplementary Fig. 1). The slight warming observed in Tx15d could potentially be due to the smoothing effect caused by averaging over a longer period and the increase in daily average summer temperature over the MUS[6]. Despite global warming has increased the intensity of heat extremes nearly everywhere across the globe[2], there has been virtually no significant change in the intensity of heat extremes over the MUS. Notable, Tx5d trends exhibit substantial deviations when compared with trends in other regions globally (Supplementary Fig. 3). The trends in the majority of grid cells across the MUS lie in the lower end of the global trends distribution (across 60S–90N), while the regional average trends fall below the 25th percentile of this distribution.

The warming of heat extremes in WEU on the other hand has remarkably accelerated in recent decades, with particularly pronounced warming across France, Germany, and northern Italy (Fig. 1). In the past 43 years (1979–2021), Tx5d has warmed >3 °C, which corresponds to a rate of increase of ~4 °C per °C GMST warming (Fig. 1c, d). While differences exist in the spatial distribution of trends and their amplitudes, warming trends in heat extremes over WEU are consistent across the observational datasets (Supplementary Fig. 1). Moreover, WEU has experienced a similar rate of warming of heat extremes of different time scales (TXx, Tx5d, and Tx15d) since 1951, suggesting an increase in both short-term temperature peaks and the sustained intensity of the high temperatures over a span of several weeks (Supplementary Fig. 1). We also observe an increasing trend in Tn5d intensity over WEU since 1979, with a rate of ~0.4 °C/decade, which is substantially smaller than for Tx5d. Nevertheless, this warming trend of the warmest nights Tn5d is nearly double the one observed in the MUS (Supplementary Fig. 2a, b). The 5 hottest days and warm nights do not necessarily co-occur but often strongly overlap and their observed year-to-year variations are highly correlated. Thus, the weaker warming trend of Tn5d than Tx5d in WEU suggests a tendency towards an enhanced diurnal temperature range, whereas in the MUS the weak Tn5d warming trend along with a weak Tx5d cooling trend points towards a reduction of the diurnal temperature range in the correspond warmest pentad.

The warming trends observed in WEU are particularly notable in comparison to trends observed in other regions worldwide (Supplementary Fig. 3). The magnitude of the warming trends across a substantial portion of WEU exceeds the trends observed in the majority of land areas globally, with the regional average warming surpassing the third quartile of the global gridded trend distribution.

Observed trends in both the MUS and WEU are outside 95% range of models. We explore initial-condition large ensembles (LEs) generated with CESM2 and a multi-model ensemble (MME) from Coupled Model Intercomparison Project 6 (CMIP6) under historical and Shared Socioeconomic Pathways 3-7.0 (SSP3-7.0) scenario (2015–2021) forcings to examine how well climate models simulate the observed heat extreme trends over the MUS and WEU (*refer to "Data and Methods" for more details)*. Regional climate projections are strongly affected by internal variability in the climate system[31,38] particularly for extremes[34], but LEs can help isolate the forced signal from internal variability and provide insight into the range of uncertainties if simulations reproduce the observed trends and related processes[38].

The regional average Tx5d trends in the MUS during 1979–2021 fall outside the 95% range of both CESM2 LE and CMIP6 MME (Fig. 2a). When considering the distribution of simulated trends as a whole, none of the members from CESM2 LE simulates cooling trends over the MUS. Instead, they exhibit warming trends across the region with a signal-to-noise ratio greater >1 (Fig. 2a and Supplementary Fig. 4). CESM2 ensemble mean shows warming of ~3 °C (with a range of 1.5–5 °C) and CMIP6 MME mean exhibits warming of ~2 °C (with a range of 0.5–4 °C) since 1979, while observations show a cooling of Tx5d by 0.25 °C. Similarly, even the observed weak warming trend in Tn5d is at the very low end of the CMIP6 MME range, while all CESM2 LE members display considerably stronger warming trends in Tn5d (Supplementary Fig. 2a).

The differences between observed and simulated trends are even larger when they are expressed as Tx5d trends per degree of global warming (Fig. 2b). The observed trends in the MUS are substantially below the 5th percentile of the trend distribution in CMIP6 MME and only one member from MPI-ESM1 captures the observed trend. Notably, observed trends are much lower than the entire distribution of trends simulated by CESM2 LE (Fig. 2b). The deviation of observed trends from CESM2 LE and CMIP6 MME is particularly pronounced in the southern part of MUS, where cooling trends are more evident (Supplementary Fig. 5). The long-term observed Tx5d trend starting in 1951 deviates even stronger from the model range (Supplementary Fig. 6). None of the members from both CESM2 LE and CMIP6 MME reach the cooling rate evident in ERA5 (Supplementary Fig. 6). Our analysis reveals similar results for TXx and Tx15d.

In contrast to MUS, the Tx5d trends over WEU fall within both the CESM2 LE and CMIP6 MME range, but are at the very high end of the simulated trends (Fig. 2c, d). The observed Tx5d trends vary in space over WEU, and lie above the ensemble mean of CESM2 LE and far above the ensemble mean of the CMIP6 MME (Fig. 2c). The CESM2 LE and CMIP6 MME simulate a Tx5d warming between ~1.5 and 3.5 °C and between ~0.5 and 3.5 °C, respectively, since 1979 compared to >3 °C in observations and reanalysis. Notably, observed Tx5d trends per °C global warming

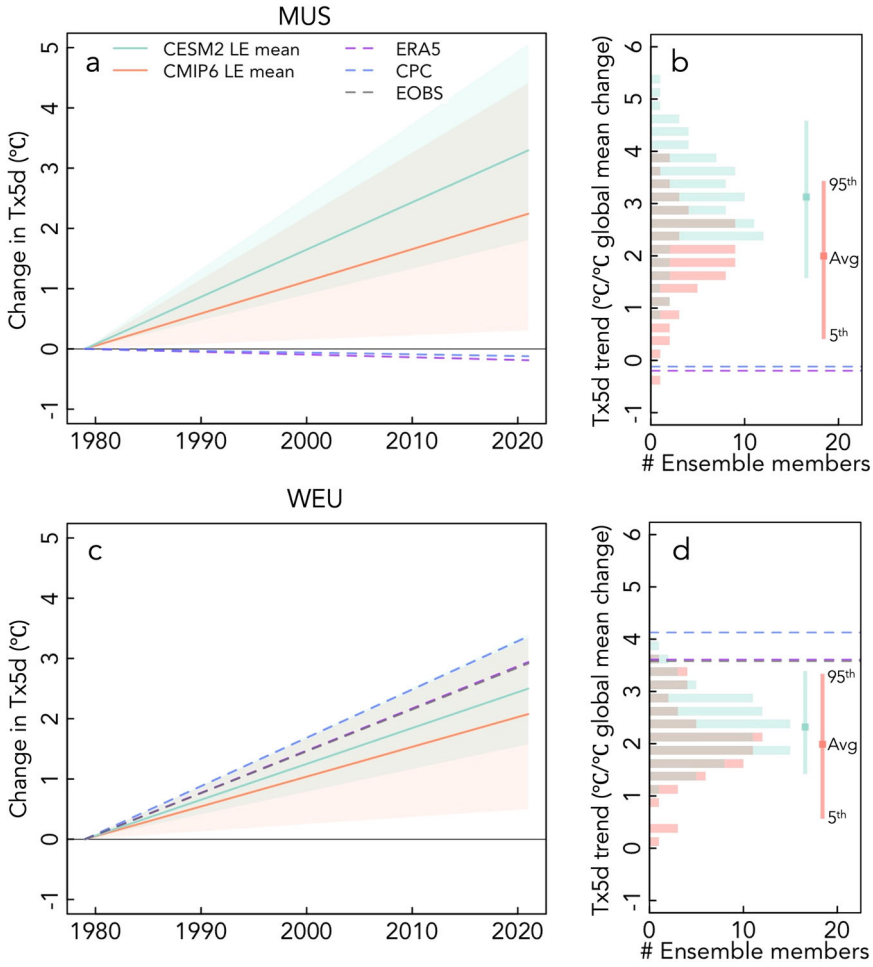

Fig. 2 Simulated vs observed trends in the intensity of Tx5d. a The yearly change in Tx5d (°C) over the MUS since 1979. The light green and orange shading represents the uncertainty range (95%, i.e., 5th to 95th percentile) across members of the CESM2 LE and CMIP6 MME, respectively. **b** Distribution of Tx5d trends, accounting for climate models' sensitivity to GMST changes, over the MUS. The horizontal colored lines indicate the trends in observations and ERA5 reanalysis. The vertical teal and orange lines represent the 5th-mean-95th percentile values of the trend distributions. **c**, **d** Same as panels **a**, **b**, respectively, but for WEU.

stand out above the 95th percentile of trend distribution simulated by both CESM2 and CMIP MME (Fig. 2d). None of the ensemble members capture the observed warming trend shown by CPC and very few of the one by ERA5 and EOBS. The mismatch between observed and almost all simulated trends is particularly noticeable in the central WEU including Germany and France, where warming trends are remarkably high (Supplementary Fig. 5). However, the lower warming rate of Tn5d compared to Tx5d, results in the observed trend in regional Tn5d falling well within and even below the median of both the CESM2 LE and CMIP6 MME range (Supplementary Fig. 2b).

Both CESM2 LE and CMIP6 MME show substantial uncertainties in Tx5d trends owing to internal variability over WEU and the MUS (Fig. 2). Although each member in the CESM2 LE has identical external forcing, the uncertainty range (95%) in trends over WEU shows a large range of Tx5d trends between 1.5 and 3.5 °C since 1979. This divergence of linear trends induced by internal variability is even more pronounced over the MUS, with uncertainties approximately twice as large as those over WEU in CESM2 LE and even 1.5x larger than those over WEU in CMIP6 MME. However, these irreducible uncertainties induced by internal variability inherent in the climate system undermine the predictability of regional heat extremes trends and the performance of climate models in simulating observed climate[34].

Circulation dampens heat extremes trends over the MUS and amplifies over WEU. Several possible explanations have been proposed to explain observed cooling in the MUS. Previous studies have investigated the role of various factors including aerosol[7], natural variability[8], and agricultural activities such as the expansion of agriculture in the early 20th century and increased irrigation in the mid-century[9,10]. Conversely, over WEU, the remarkable acceleration in heat extremes over recent decades has been linked to changes in atmospheric circulation[19].To better understand the observed trends, we here employ a dynamic adjustment[37,39] approach to quantify the contributions of circulation- and thermodynamic-induced changes to observed trends in these regions. Here, we use linearly detrended geopotential height at 500 hPa pressure level (Z500) within circulation domains as an atmospheric circulation proxy to capture heat extreme variations driven by circulation changes in these regions. We detrended Z500 by subtracting the daily global-mean Z500 value from the daily Z500 at each grid and each time step before temporally averaging across the days experiencing heat extremes. This allows us to remove forced components from Z500 to isolate the dynamic component of heat extremes related solely to Z500 variations in the circulation domain[40]. We apply statistical learning principles and employ regularized ridge regression to establish the physical relationship

between Z500 and heat extremes (*Refer to* "*Data and Methods*" for more details).

We find that circulation substantially dampened the observed trends in regionally-averaged Tx5d in the MUS (Fig. 3a, b). Circulation induced a cooling trend of ~0.2 °C /decade over the MUS, with notably strong circulation-induced cooling trends in the lower MUS (Figs. 3a and 4a, b). When expressed per °C global warming, the circulation-induced trends correspond to ~1 °C cooling in Tx5d in the MUS (Fig. 3b). In contrast, forced warming (hereafter referred to as "*thermodynamic-induced*") is much weaker over the MUS, potentially due to land use changes and aerosols. Consequently, circulation-driven cooling trends are strong enough to reverse weak thermodynamic-induced warming, resulting in an overall cooling trend. Cooling in the MUS has been documented for an even longer period 1910–2014 and primarily attributed to the extensive expansion of irrigation during the latter half of the 20th century[9]. Furthermore, the overall increase in albedo resulting from the conversion of natural vegetation to croplands has influenced primarily hot days and exhibits insignificant cooling effects.

Notably, long-duration heat extremes, such as Tx15d, show relatively stronger warming from thermodynamics, as well as stronger cooling induced by circulation, in comparison to Tx5d (Supplementary Fig. 7). This suggests that our method may be somewhat conservative in capturing the complete circulation-induced trends, as short-scale temperature extremes exhibit more pronounced feedbacks between land and atmosphere, and in general a stronger manifestation of internal variability. Another possible explanation could be the limited influence of local-scale factors, such as irrigation or land conversion, on exceptionally hot

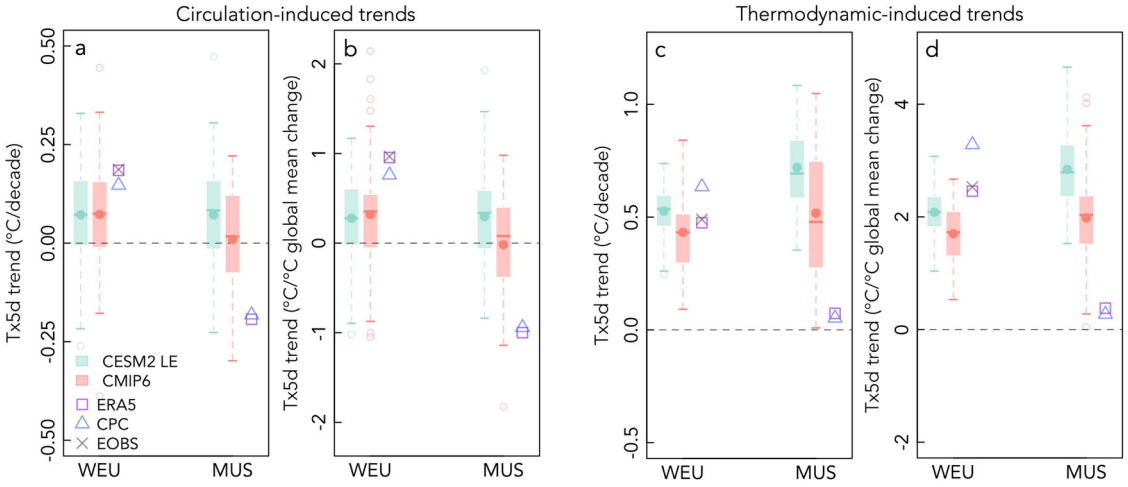

Fig. 3 Contributions of circulation- and thermodynamic-induced trends to Tx5d trends. a Proportion of Tx5d trends attributed to circulation changes over WEU and the MUS in large ensembles, observations, and reanalysis. **b** Circulation-induced trends relative to changes in GMST. **c**, **d** Same as panels **a**, **b**, respectively, but show thermodynamic-induced trends.

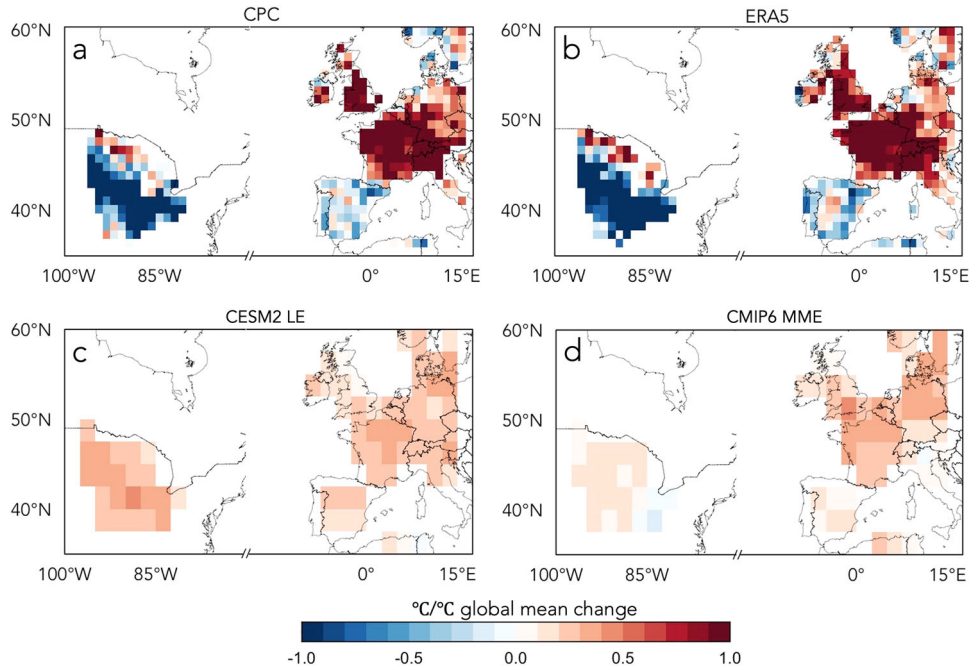

Fig. 4 Spatial distributions of circulation-induced trends. a, **b** Circulation-induced Tx5d trends as observed in CPC and ERA5 reanalysis datasets over WEU and the MUS from 1979 to 2021. **c**, **d** Average of simulated trends due to circulation changes across the ensemble members from CESM2 LE and CMIP6 MME. These trends are compared against the GMST trend.

days, as suggested by Mueller et al.[9]. We also found similar contributions from circulation and thermodynamics to long-term trends in Tx5d starting from 1951. The trends induced by circulation and thermodynamics are also consistent for Tn5d; however, their amplitudes differ (Supplementary Fig. 1a, b). Specifically, circulation changes induce a decreasing trend in Tn5d, but at a smaller rate than for Tx5d, while the trend attributable to thermodynamics is substantially greater than that observed for Tx5d. Notably, the thermodynamic trend in Tn5d is very similar for the MUS and WEU.

The cooling trends in Tx5d induced by circulation in the MUS are substantially lower than the first quartile of trend distribution from CESM LE and CMIP6 MME (Figs. 3 and 4). Notably, the mean circulation-induced trend in CESM2 LE shows positive values, and none of the ensemble members captures the observed cooling trends when expressed per °C of global warming (Figs. 3b and 4). Moreover, circulation-induced trends in observations lie at the edge of the model range and are only captured by a few individual CMIP6 MME (Fig. 3b). Overall, CMIP6 MME simulates lower circulation-induced trends (with a distribution mean of ~0) compared to CESM2 LE, resulting in relatively smaller deviations from observed trends. However, more research is needed to understand whether the couple of members from CMIP6 MME reproduce these trends for the correct underlying mechanisms.

Similar to circulation-induced trends, the observed thermodynamic-induced trends over the MUS also fall outside the entire distribution range from CESM2 LE and are only simulated by a few CMIP6 models. The mismatch between simulated and observed trends becomes more pronounced when estimating regional thermodynamic-induced trends per °C of global warming (Supplementary Fig. 9). The observed thermodynamic-induced trends for Tx15d are larger and thereby closer to the range of simulated thermodynamic-induced trends. Similar behavior is found for TXx as well, showing broad consistency with these findings.

In contrast to the MUS, over WEU circulation-induced changes contribute to an additional warming effect of ~0.2 °C/decade in Tx5d, accounting for about 1/3 of the total observed trends (Fig. 3a). The trend amplification resulting from circulation is particularly large over Germany and France, and parts of the UK (Fig. 4a, b). Nonetheless, Tx5d trends over WEU are dominated by the thermodynamic-induced corresponding to about 2/3 of the warming largely caused by external anthropogenic forcings (Fig. 3c). Specifically, thermodynamic-induced changes cause warming exceeding >0.5 °C/decade (equivalent to ~3 °C rise for each °C change in GMST) over WEU, with even stronger warming in central regions (Fig. 3c, d). When combined with the amplifying warming from circulation, this results in a warming of ~0.8 °C/decade over WEU. Notably, the contribution of circulation-induced trends is even larger for Tn5d, accounting for almost half of the observed warming trend in Tn5d. Previous studies have linked the disproportionate warming trends in WEU to various processes, including changes in soil moisture and associated land-atmosphere feedback mechanisms[29,30], as well as atmospheric dynamical changes, particularly the increase in the frequency and persistence of double jet stream states over Eurasia[19].

While circulation-induced trends closely align with the third quartile of both CESM2 LE and CMIP6 MME, they considerably exceed the third quartile when expressed per degree of global warming (Fig. 3). However, the observed thermodynamic-induced trends in time are still within the ensemble ranges, but are outside the entire distribution from CESM2 LE and at the upper end of the distribution from CMIP6 MME when expressed relative to global warming rate. Thus, some simulations capture the observed regional trend due to an overestimation of the global warming trend. As expected, the spread of the thermodynamic-induced trends is smaller than of the total trends within both ensembles and the observed trends align more closely with models. This suggests a relatively high level of confidence in the externally forced trends over WEU. However, a potential limitation is that the thermodynamic trends here are estimated as a residual from the circulation-induced contribution, thus any misrepresentation or unexplained components of the statistical dynamical adjustment model such as a lagged temperature response to certain atmospheric circulation patterns would be interpreted as a thermodynamic variation. So while we find a large contribution of circulation-induced trends in both regions, we consider this estimate as a conservative estimate.

In summary, both circulation-induced trends are at the high end of the range and thermodynamic-induced trends above the mean, which explains why together the total observed trends over WEU are at the very high end of the model range. On the contrary, in the MUS both thermodynamic and dynamic-induced trends are at the very low end of the models. Together they explain why the total trends are outside the model range. While removing the impact of internal atmospheric variability does substantially reduce the trend range, it does not fully reconcile the discrepancies between simulated and observed total trends. This suggests that care is required when interpreting the forced response in the models.

Discussion and conclusions

We here investigate trends for two selected regions with very unusual behavior. Heat extremes over the MUS and WEU have received much attention from media, societies, and the climate science community due to their remarkably low and high trends in heat extremes intensity since 1979. Here, we demonstrate that circulation played a crucial role and amplified the trends in heat extreme intensity over WEU and dampened or even reversed the trends over the MUS. Over the MUS, circulation dampens the trend in the intensity of the hottest five-day period (Tx5d) by 0.2 °C/decade or 1 °C per degree of global warming. Consequently, the cooling trend resulting from circulation changes is strong enough to reverse the weak thermodynamic-induced warming trend, leading to an overall weak cooling trend in heat extremes over the MUS. The relatively weak thermodynamic warming trend over the MUS may be due to the land use changes, irrigation, and aerosol forcing[7–9]. However, the cooling effects of these local factors are primarily limited to short-duration temperature peaks or exceptionally hot days, and their influence diminishes for longer-duration events such as Tx15d. Moreover, the stronger manifestation of internal variability on short-duration heat extremes poses challenges in attributing the complete circulation-induced trends. Consequently, the remaining component of circulation-induced cooling offsets the thermodynamic warming, resulting in a lower thermodynamic-induced trend in Tx5d or even in TXx. We also show that particularly the contributions of circulation-induced trends to Tn5d trends are consistent with those observed for heat extremes such as Tx5d, thus highlighting the robustness of the methods employed here.

Even after accounting for the circulation-induced trends, coupled climate models still exhibit a wide range of thermodynamic-induced trends over the MUS, with observations being at the lower end of the ensemble range. Thus, while accounting for circulation explains part of the difference in trends between observations and models, it does not fully reconcile observations with all models. This may be due to the fact that our method does not remove all of the circulation-induced trends, or that some of the relevant forces such as irrigation, land use, land management, or aerosol are not accurately represented or to an overestimated thermodynamic

model response. Overall it suggests that the projected trends in heat extremes over the MUS remain uncertain.

In contrast to the MUS, circulation changes in WEU induce a warming trend in heat extremes of ~0.2 °C/decade or 1 °C per degree of global warming, contributing to at least 1/3 of the observed trend. This warming trend due to circulation is similar to that observed in the MUS but occurs in the opposite direction. The observed circulation-induced warming is at the high end of the model range, while the thermodynamic-induced warming exceeds the CMIP6 and CESM2-LE ensemble averages. The combination of these two effects contributes to the fact that the total observed trend is at the high end of the model range over WEU, as also highlighted in previous studies[5,41].

At the global scale, trends in heat extremes over most regions fall within the 95% range of CMIP6 MME and CESM2 LE, but nevertheless, ~40% and ~28% of the land area fall outside CMIP6 MME and CESM2 LE ranges, respectively. Hence, it should be noted that these two regions have been selected as two illustrative regions with unusual trends in heat extremes. However, these trends are not the most extreme globally. We have deliberately not selected the regions with the highest trends and discrepancies with large ensembles to prevent potential selection bias. Also, while certain regions show more pronounced decreasing trends compared to those observed in the MUS, these trends are localized to very small geographical extents and lack regional coherence beyond their specific locations. A better understanding of historical heat extreme trends and their implications for the future is critical for both regions. The MUS region is primarily dominated by the most productive agricultural land in the country, while the steep rise in heat extremes over WEU has already caused devastating impacts in the past.

We find that unusual trends in circulation strongly affected recent trends in heat extremes. However, the key question remains: to what extent do these trends represent unforced internal variability or a forced response in circulation? The observed circulation-induced trends in WEU are at the higher end of the climate models' range, consistent with previous studies on broader patterns of decadal variations in boreal summer atmospheric circulation[42] and multidecadal variability in the winter season, particularly in Europe[43]. This can be potentially due to various reasons such as erroneous representations of the circulation response to either external climate forcing, or underestimated internal variability, or both, and their dependence on model parameterizations. Model evidence remains inconclusive regarding whether these trends result from unforced internal variability, or are they a response to external influences[19,43]. Nevertheless, gaining a more advanced understanding of the underlying physical mechanisms would be helpful to more accurately assess whether circulation changes primarily result from internal variability or external forcings. Additionally, process studies isolating the circulation response to warming patterns via analogs of internal variability such as dynamical adjustment or targeted climate model experiments can provide valuable insights for attributing these trends to their origins, although disentangling forced circulation change remains challenging[44].

Nonetheless, our results imply that if circulation-induced trends are externally forced, WEU may continue experiencing a rise in the intensity of heat extreme as they can further intensify in the warmer world. On the one hand, these cooling trends may continue dampening the warming trends over the MUS, implying favorable conditions for agriculture activities, as maximum temperatures may not substantially rise in the coming decades. But, if these trends are a result of unforced internal variability inherent in the climate system, they likely reverse in the coming decades and thus lead to slow down the rise of heat extremes over WEU and warmer conditions over the MUS. Further, knowledge of uncertainties in processes that derive these unusual trends over these regions would be crucial to constrain model projections[36] on a regional scale and to design effective adaptation and resilience plans.

Data and methods

Data. We used daily maximum temperature (TX) data from multiple observational sources and reanalysis to ensure the robustness of our findings. Specifically, we considered TX from CPC (1979–2021), EOBS (1951-2020), GHCNDEX (1951–2021), HADEX3 (1951–2018), and from ERA5 reanalysis during 1951–2021. Although the reanalysis TX dataset has been available since 1951, we primarily focused on heat extremes trends from 1979 onwards due to the availability of observational data. The EOBS dataset covers only the European domain, and the GHCNDEX and HADEX3 datasets contain annual maximum TX. We also used geopotential height at 500 hPa pressure level (Z500) from the ERA5 reanalysis dataset to dynamically adjust the observed trends. The trends in heat extremes are calculated using Theil-Ssen's slope estimator.

Climate model simulations. We also utilized initial-condition large ensembles from CESM2 and a set of CMIP6 climate models under historical forcings from 1951–2014 and Shared Socioeconomic Pathways 370 (SSP370) until 2021. The CESM2 large ensemble comprises 89 members, while the CMIP6 multimodal large ensembles consist of 30 members from MPI-ESM, 10 members each from CanESM5, MIROC-ES2L, 13 members from UKESM1, and one run each from GFDL-ESM4, CMCC-ESM2 and NorESM2. Additionally, We utilized pre-industrial simulations from CESM2 for 2070 years to train the regularized regression model used in dynamical adjustment analysis.

Study and circulation domains. We area-weighted averaged TX over the MUS (Melillo et al.[45]) and WEU (−10 to +15E, 36–60 N) (shown by blue polygons in Supplementary Fig. 10) to estimate the regional average heat extremes. Our analysis primarily focuses on the 5-day maximum of TX (Tx5d), but the 1-day maximum (TXx) and hottest five-day period (Tx15d) are also considered to ensure the insensitivity of analysis to a specific heat metric. We define the circulation over relatively larger domains over these regions. Circulations are characterized by geopotential height at 500 hPa pressure level (Z500) over the [116 to 60 W, 16–68 N] for the MUS and over the [−30 to +35E, 16–80 N] for WEU (see red rectangles in Supplementary Fig. 10). We also validated our results with a circulation of slightly different size and largely found that results are not much sensitive to the size of the circulation domain.

Dynamical adjustment. The dynamical adjustment approach is widely used to quantify the proportion of variability of a target variable (here heat extremes) that can be attributed to changes in the atmospheric circulation while assuming that other factors remain constant[37,39]. Precisely, this approach decomposes heat extremes into two distinct components: a dynamical (or circulation) component associated with changes in atmospheric circulation, and a residual component that predominantly represents contributions from externally forced changes. In this study, we use principles from statistical learning and employ a regularized ridge regression to establish a physical relationship between the heat extremes and dominant atmospheric circulation pattern (here, Geopotential potential height at 500 hPa (Z500)). This relationship is expressed through the following equation:

$$T_N = f\left(Z500_{N\times P}\right) \quad (1)$$

where T is a target variable of length N (years), and $Z500$ is a predictor matrix of size $N \times P$, where P is the number of grid cells

within the circulation domain. f is a regularized ridge regression model. During the training phase on the control runs, a k-fold cross-validation scheme is employed to tune the regression model and prevent overfitting.

Importantly, our statistical model is trained on 2070-year pre-industrial simulations from CESM2 rather than transient climate simulation to avoid any false learning of the regression model due to forced warming. We detrended Z500 by subtracting the daily global-mean Z500 value from the daily Z500 at each grid cell and each time step before temporally averaging across the days experiencing heat extremes[40]. This detrending process removes the influence of thermal expansion of the troposphere, primarily driven by anthropogenic global warming, on Z500.

Subsequently, we employed the detrended Z500 as input for the trained regression model throughout the study period. This step allows us to derive the dynamical components or predicted values of heat extremes, solely driven by changes in Z500 across the circulation domain. It's important to note that the dynamic component encapsulates the influence of atmospheric circulation changes, encompassing both direct effects like advection and indirect effects such as local effects that are implied by a given circulation regime[28]. The residual component is expected to contain the externally forced component, but also local feedback due to soil moisture-atmosphere interactions[46]. However, this does not imply that circulation changes are solely due to internal variability as external forcing can also affect atmospheric circulation and subsequently, the characteristics of heat extremes[40]. In such scenarios, our method may potentially overestimate the influence of internal variability on circulation changes. Conversely, circulation changes may be underestimated if the detrending technique inadvertently removes the part of circulation changes attributable to internal variability while eliminating the effects of forced thermal expansion of the troposphere.

Data availability

All datasets used in this study are publicly available. Observed temperature datasets from CPC are available at https://psl.noaa.gov/data/gridded/data.cpc.globaltemp.html, from EOBS at https://www.ecad.eu/download/ensembles/download.php#datafiles, from GHCNDEX at https://climatedataguide.ucar.edu/climate-data/ghcndex-gridded-temperature-and-precipitation-climate-extremes-indices-climdex-data, and from HADEX3 at https://www.metoffice.gov.uk/hadobs/hadex3/. The reanalysis ERA5 datasets are available at https://cds.climate.copernicus.eu/#!/search?text=ERA5. The CESM2 LE simulations are accessible from the climate data repository at ETH Zurich. The CMIP6 MME simulations can be accessed at https://esgf-node.llnl.gov/projects/cmip6/.

Code availability

The R scripts developed for the analysis are available from the corresponding author and are also available at: https://doi.org/10.5281/zenodo.10040950

Received: 22 June 2023; Accepted: 8 November 2023;
Published online: 23 November 2023

References

1. Gillett, N. P. et al. Constraining human contributions to observed warming since the pre-industrial period. *Nat. Clim. Chang.* **11**, 207–212 (2021).
2. Seneviratne, S. I. et al. in *Climate Change 2021: The Physical Science Basis*. Contribution of Working Group I to the Sixth Assessment Report of the Intergovernmental Panel on Climate Change. pp. 1513–1766 https://doi.org/10.1017/9781009157896.013 (Cambridge University Press, Cambridge, United Kingdom and New York, NY, USA, 2021).
3. Perkins-Kirkpatrick, S. E. & Lewis, S. C. Increasing trends in regional heatwaves. *Nat. Commun.* **11**, 3357 (2020).
4. Zhang, H. et al. Unequal urban heat burdens impede climate justice and equity goals. *The Innovation* **4**, 100488 (2023).
5. Van Oldenborgh, G. J. et al. Attributing and projecting heatwaves is hard: we can do better. *Earth's Future* **10**, e2021EF002271 (2022).
6. Basso, B., Martinez-Feria, R. A., Rill, L. & Ritchie, J. T. Contrasting long-term temperature trends reveal minor changes in projected potential evapotranspiration in the US Midwest. *Nat. Commun.* **12**, 1476 (2021).
7. Mascioli, N. R., Previdi, M., Fiore, A. M. & Ting, M. Timing and seasonality of the United States 'warming hole'. *Environ. Res. Lett.* **12**, 034008 (2017).
8. Partridge, T. F. et al. Spatially distinct seasonal patterns and forcings of the U.S. warming hole. *Geophys. Res. Lett.* **45**, 2055–2063 (2018).
9. Mueller, N. D. et al. Cooling of US midwest summer temperature extremes from cropland intensification. *Nat. Clim. Chang.* **6**, 317–322 (2016).
10. Nikiel, C. A. & Eltahir, E. A. B. Summer climate change in the midwest and great plains due to agricultural development during the twentieth century. *J. Clim.* **32**, 5583–5599 (2019).
11. Ellenburg, W. L., McNider, R. T., Cruise, J. F. & Christy, J. R. Towards an understanding of the twentieth-century cooling trend in the Southeastern United States: biogeophysical impacts of land-use change. *Earth Interact.* **20**, 1–31 (2016).
12. Meehl, G. A., Arblaster, J. M. & Branstator, G. Mechanisms contributing to the warming hole and the consequent U.S. East-west differential of heat extremes. *J. Clim.* **25**, 6394–6408 (2012).
13. Fischer, E. M., Sippel, S. & Knutti, R. Increasing probability of record-shattering climate extremes. *Nat. Clim. Chang.* **11**, 689–695 (2021).
14. Jurg, Luterbacher, Daniel, Dietrich, Elena, Xoplaki, Martin, Grosjean & Heinz, Wanner European seasonal and annual temperature variability, trends, and extremes since 1500. *Science (1979)* **303**, 1499–1503 (2004).
15. Schar, Christoph et al. The role of increasing temperature variability in European summer heatwaves. *Nature* **427**, 328–332 (2004).
16. Fischer, E. M., Seneviratne, S. I., Lüthi, D. & Schär, C. Contribution of land-atmosphere coupling to recent European summer heat waves. *Geophys. Res. Lett.* **34**, (2007).
17. Seneviratne, S. I., Lüthi, D., Litschi, M. & Schär, C. Land-atmosphere coupling and climate change in Europe. *Nature* **443**, 205–209 (2006).
18. Della-Marta, P. M. et al. Summer heat waves over western Europe 1880-2003, their relationship to large-scale forcings and predictability. *Clim. Dyn.* **29**, 251–275 (2007).
19. Rousi, E., Kornhuber, K., Beobide-Arsuaga, G., Luo, F. & Coumou, D. Accelerated western European heatwave trends linked to more-persistent double jets over Eurasia. *Nat. Commun.* **13**, 3851 (2022).
20. Van Oldenborgh, G. J. et al. Western Europe is warming much faster than expected. *Clim. Past* **5** www.clim-past.net/5/1/2009/ (2009).
21. Lorenz, R., Stalhandske, Z. & Fischer, E. M. Detection of a climate change signal in extreme heat, heat stress, and cold in Europe from observations. *Geophys. Res. Lett.* **46**, 8363–8374 (2019).
22. Mann, M. E. et al. Influence of anthropogenic climate change on planetary wave resonance and extreme weather events. *Sci. Rep.* **7**, 1–12 (2017).
23. Kautz, L. A. et al. Atmospheric blocking and weather extremes over the Euro-Atlantic sector-a review. *Weather Clim. Dyn.* **3**, 305–336 (2022).
24. Dong, B., Sutton, R. T. & Shaffrey, L. Understanding the rapid summer warming and changes in temperature extremes since the mid-1990s over Western Europe. *Clim. Dyn.* **48**, 1537–1554 (2017).
25. Dong, B., Sutton, R. T., Shaffrey, L. & Harvey, B. Recent decadal weakening of the summer Eurasian westerly jet attributable to anthropogenic aerosol emissions. *Nat. Commun.* **13**, 1148 (2022).
26. Boé, J., Terray, L., Cassou, C. & Najac, J. Uncertainties in European summer precipitation changes: role of large scale circulation. *Clim. Dyn.* **33**, 265–276 (2009).
27. Patterson, M. North-West Europe hottest days are warming twice as fast as mean summer days. *Geophys. Res. Lett.* **50**, e2023GL102757 (2023).
28. Terray, L. A dynamical adjustment perspective on extreme event attribution. *Weather Clim. Dyn.* **2**, 971–989 (2021).
29. Sousa, P. M. et al. Distinct influences of large-scale circulation and regional feedbacks in two exceptional 2019 European heatwaves. *Commun. Earth Environ.* **1**, 48 (2020).
30. Stegehuis, A. I. et al. Early summer soil moisture contribution to Western European Summer warming. *J. Geophys. Res. Atmos.* **126**, e2021JD034646 (2021).
31. Deser, C., Knutti, R., Solomon, S. & Phillips, A. S. Communication of the role of natural variability in future North American climate. *Nat. Clim. Change* **2**, 775–779 (2012).
32. Banerjee, A., Polvani, L. M. & Fyfe, J. C. The United States "warming hole": quantifying the forced aerosol response given large internal variability. *Geophys. Res. Lett.* **44**, 1928–1937 (2017).
33. Deser, C., Phillips, A. S., Alexander, M. A. & Smoliak, B. V. Projecting North American climate over the next 50 years: uncertainty due to internal variability. *J. Clim.* **27**, 2271–2296 (2014).

34. Fischer, E. M., Beyerle, U. & Knutti, R. Robust spatially aggregated projections of climate extremes. *Nat. Clim. Chang.* **3**, 1033–1038 (2013).
35. Sutton, R. T. & Dong, B. Atlantic ocean influence on a shift in European climate in the 1990s. *Nat. Geosci.* **5**, 788–792 (2012).
36. Tokarska, K. B. et al. Pastwarming trend constrains future warming in CMIP6 models. *Sci. Adv.* **6**, eaaz9549 (2020).
37. Sippel, S. et al. Uncovering the forced climate response from a single ensemble member using statistical learning. *J. Clim*. https://doi.org/10.1175/JCLI-D-18-0882.s1 (2019).
38. Deser, C. et al. Insights from Earth system model initial-condition large ensembles and future prospects. *Nat. Clim. Chang.* **10**, 277–286 (2020).
39. Deser, C. & Phillips, A. S. Forced and internal components of winter air temperature trends over North America during the past 50 years: mechanisms and implications. *J. Clim*. **29**, 2237–2257 (2016).
40. Zhuang, Y., Fu, R., Santer, B. D., Dickinson, R. E. & Hall, A. Quantifying contributions of natural variability and anthropogenic forcings on increased fire weather risk over the western United States. *Proc. Natl Acad. Sci. USA* **118**, e2111875118 (2021).
41. Vautard, R. et al. Human contribution to the record-breaking June and July 2019 heatwaves in Western Europe. *Environ. Res. Lett.* **15**, 094077 (2020).
42. Teng, H., Leung, R., Branstator, G., Lu, J. & Ding, Q. Warming pattern over the northern hemisphere midlatitudes in Boreal summer 1979–2020. *J. Clim.* **35**, 3479–3494 (2022).
43. Blackport, R. & Fyfe, J. C. *Climate models fail to capture strengthening wintertime North Atlantic jet and impacts on Europe. Sci Adv*. **8**, eabn311(2022).
44. Zappa, G. Regional climate impacts of future changes in the mid–latitude atmospheric circulation: a storyline view. *Curr. Clim. Change Rep.* **5**, 358–371 (2019).
45. Melillo, J. M., Richmond, T. C. & Yohe, G. W. Eds. Highlights of Climate Change Impacts in the United States: The Third National Climate Assessment. U.S. Global Change Research Program, 137 pp. (2014).
46. Merrifield, A., Lehner, F., Xie, S. P. & Deser, C. Removing circulation effects to assess central U.S. land-atmosphere interactions in the CESM large ensemble. *Geophys. Res. Lett.* **44**, 9938–9946 (2017).

Acknowledgements

All authors acknowledge funding from the European Union's Horizon 2020 research and innovation program (XAIDA, grant number-101003469). The statistical analysis and figures are generated by freely available R statistical software.

Author contributions

All authors conceived and designed the study. J.S. collected the data and performed the analyses. All authors were involved in discussions of the results. J.S. wrote the manuscript with feedback from S.S. and E.M.F.

Competing interests

The authors declare no competing interests.

Additional information

Supplementary information The online version contains supplementary material available at https://doi.org/10.1038/s43247-023-01096-7.

Correspondence and requests for materials should be addressed to Jitendra Singh.

Peer review information *Communications Earth & Environment* thanks the anonymous reviewers for their contribution to the peer review of this work. Primary handling editors: Akintomide Akinsanola, Heike Langenberg. A peer review file is available.

Reprints and permission information is available at http://www.nature.com/reprints

Publisher's note Springer Nature remains neutral with regard to jurisdictional claims in published maps and institutional affiliations.